Stabilization of U $5f^2$ configuration in UTe_2 through U $6d$ dimers in the presence of Te2 chains

Denise S. Christovam,[1] Martin Sundermann,[1,2] Andrea Marino,[1] Daisuke Takegami,[1,*] Johannes Falke,[1] Paulius Dolmantas,[1] Manuel Harder,[3,4] Hlynur Gretarsson,[2,5] Bernhard Keimer,[5] Andrei Gloskovskii,[2] Maurits W. Haverkort,[6] Ilya Elfimov,[7] Gertrud Zwicknagl,[1,8] Alexander V. Andreev,[9] Ladislav Havela,[10] Mitchell M. Bordelon,[11] Eric D. Bauer,[11] Priscila F. S. Rosa,[11] Andrea Severing,[1,12] and Liu Hao Tjeng[1]

[1]*Max Planck Institute for Chemical Physics of Solids, Nöthnitzer Straße 40, 01187 Dresden, Germany*

[2]*PETRA III, Deutsches Elektronen-Synchrotron DESY, Notkestraße 85, 22607 Hamburg, Germany*

[3]*Department of Physics, Universität Hamburg, Notkestraße 9-11, 22607 Hamburg, Germany*

[4]*European XFEL GmbH, Holzkoppel 4, 22869 Schenefeld, Germany*

[5]*Max Planck Institute for Solid State Research, Heisenbergstraße 1, 70569 Stuttgart, Germany*

[6]*Institute for Theoretical Physics, Heidelberg University, Philosophenweg 19, 69120 Heidelberg, Germany*

[7]*Quantum Matter Institute, University of British Columbia, Vancouver, British Columbia, Canada V6T 1Z4*

[8]*Institute for Mathematical Physics, Technische Universität Braunschweig, D-38106 Braunschweig, Germany*

[9]*Institute of Physics, Academy of Sciences of the Czech Republic, Na Slovance 1999/2, 182 21 Prague 8, Czech Republic*

[10]*Department of Condensed Matter Physics, Faculty of Mathematics and Physics, Charles University, Ke Karlovu 5, 121 16 Prague 2, Czech Republic*

[11]*Los Alamos National Laboratory, Los Alamos, New Mexico 87545, USA*

[12]*Institute of Physics II, University of Cologne, Zülpicher Straße 77, 50937 Cologne, Germany*

(Received 29 January 2024; accepted 23 August 2024; published 16 September 2024)

We investigate the topological superconductor candidate UTe_2 using high-resolution valence-band resonant inelastic x-ray scattering at the U $M_{4,5}$ edges. We observe atomiclike low-energy excitations that support the correlated nature of this unconventional superconductor. These excitations originate from the U $5f^2$ configuration, which is unexpected since the short Te2-Te2 distances exclude Te2 being 2−. By utilizing the photoionization cross-section dependence of the photoemission spectra in combination with band structure calculations, we infer that the stabilization of the U $5f^2$ configuration is due to the U $6d$ bonding states in the U dimers acting as a charge reservoir. Our results emphasize that the description of the physical properties should commence with a $5f^2$ ansatz.

DOI: 10.1103/PhysRevResearch.6.033299

I. INTRODUCTION

UTe_2 is a recently discovered odd-parity superconductor that emerged as a promising candidate for topological superconductivity. Since the discovery of superconductivity in 2019 [1–3], a plethora of experimental and theoretical studies has boosted our understanding of this intriguing material (see, e.g., [4] and references therein). Two central issues, however, remain unsettled even under ambient conditions. First, numerous proposals exist for the superconducting order parameter, which include either multicomponent [5–7] or single-component representations [8–11]. Second, whether the local uranium multiplet configuration is U^{3+} ($5f^3$) or U^{4+} ($5f^2$) remains a matter of fierce debate, experimentally [12–19] as well as theoretically [6,20–22]. UTe_2 crystallizes in the orthorhombic *Immm* structure (space group 71) [23], as depicted in Figs. 1(a) and 1(b), and exhibits superconductivity with a critical temperature (T_c) of 2.1 K in the latest generation of samples grown through the molten salt technique [24]. The upper critical field is anisotropic and much higher than the Pauli limit expected for even-parity superconductors [4,25]. The NMR Knight-shift drop at T_c is also much smaller than expected for an even-parity superconducting state [26]. Importantly, the ground state of UTe_2 can be easily tuned through external parameters. Re-entrant superconductivity has been observed in magnetic fields applied either along b or between the b and c axes [27,28]. Hydrostatic pressure suppresses T_c at first, but above a pressure of only 0.3 GPa, two superconducting transitions are identified. At even higher pressures, antiferromagnetic order is observed [29]. More recent investigations show that UTe_2 undergoes a structural phase transition to a body centered tetragonal phase between 3 and 5 GPa [14,30–32].

A key challenge in understanding anisotropic properties, as well as their dependence on tuning parameters, is finding the appropriate ansatz for describing such a complex f-electron system, situated at the border between localization and itineracy. Electronic structure investigations are essential to determine the extent to which local physics persists and to identify the electronic configuration that governs the

*Present address: Department of Applied Physics, Waseda University, Shinjuku, Tokyo 169-8555, Japan.

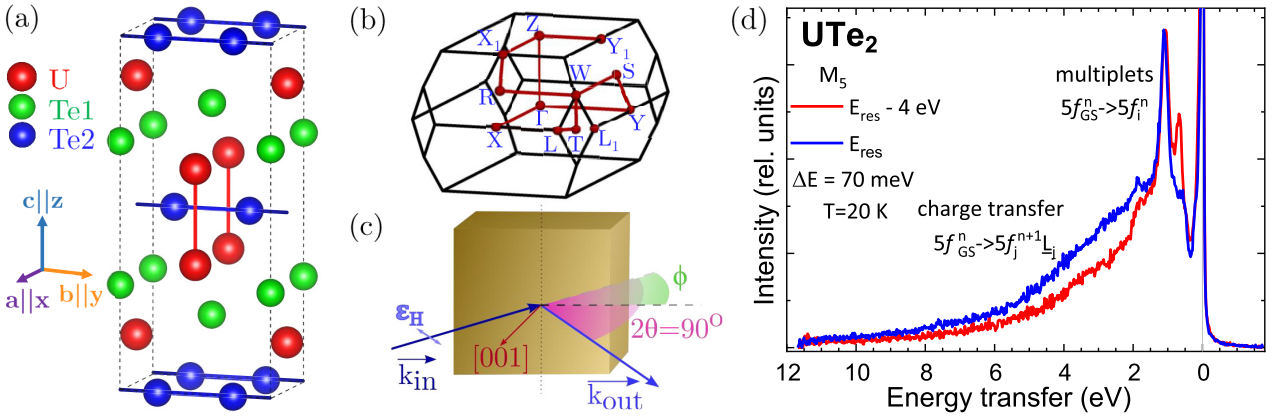

FIG. 1. Crystal structure of UTe_2 (a). First Brillouin zone of UTe_2 showing the main high-symmetry paths (b). Geometry of RIXS experiment, with scattering angle 2θ, sample angle ϕ, wave vector of incoming and outgoing x-rays $\vec{k}_{in,out}$, and ϵ_H horizontal polarization (c). M_5-edge valence band RIXS spectrum of UTe_2 in a large energy window showing, in addition to elastic scattering, multiplet and charge transfer excitations (d).

unusual low-temperature properties. UTe_2 has been investigated by several groups using various experimental methods, but the interpretation of the data does not yield a uniform picture [12–19].

Generally, in uranium-based intermetallics several U configurations from $5f^0$ to $5f^4$ or even $5f^5$ contribute to the intermediate valent ground state [33,34], but in the presence of electron correlations, it is important to know which configuration, usually the $5f^3$ or the $5f^2$, has the strongest weight and sets the stage for the ground state symmetry; for example, Kramers doublets in case of the former and singlet states for the latter. Unfortunately, discrepancies in determining the dominant $5f$ configuration are common, as also seen in [35–40]. We believe these apparent contradictions arise from the challenge to quantitatively analyze the spectra. Very different U $4f$ core-level spectra may originate from the same averaged valence but different degrees of covalence [34]. Hence, U core-level data can be very misleading due to the complexity of the underlying many-body problem and uncertainties in the input model. This issue is particularly serious when extracting information about the electronic states from fine variations in the energy separation or intensity ratio of broad and structureless spectral features. Also, the use of extrapolation schemes [19,41] to extract expectation values from integer valent (ionic) calculations [42,43] neglects the interference terms due to configuration interaction and may thus give unreliable results [44].

Here, we choose a spectroscopic method that provides a "fingerprint," i.e., a distinctive set of strong spectral features if local f-electron physics is present and that are unique for any U $5f^n$ configuration [45]. In our previous work [46], we demonstrated that a novel setup for high-resolution valence-band (VB) resonant inelastic x-ray scattering (RIXS) at the U M_5 edge ($3d \rightarrow 5f$) in the tender x-ray regime offers sufficient resolution to reveal atomiclike low-energy excitations in UGa_2, a prototypical uranium intermetallic material. We successfully distinguished whether the main configuration is $5f^2$ or $5f^3$. The signal-to-background ratio of VB-RIXS at the U M_5 edge is high. In this study, we additionally utilize the U M_4 edge to provide yet another "fingerprint" of localized $5f$ configuration, further confirming the reliability of our method.

II. EXPERIMENT

The U $M_{4,5}$-edge RIXS experiments were conducted at the Max-Planck IRIXS endstation of the P01 beamline at Petra III/DESY (Hamburg, Germany) [47–49]. The resolution at the U M_5 edge (3.5 keV) initially was 150 meV and later improved to 70 meV. At the U M_4 edge (3.7 keV), the resolution progressed from 250 meV to 150 meV. The experimental setup is depicted in Fig. 1(c). Spectra were gathered at various incident photon energies across the absorption edges to capitalize on the energy dependence of the cross section. We will focus on the energies at the resonance maximum, E_{res}, and 4 eV below the resonance, E_{res} - 4 eV. Additional details about the experiment and sample synthesis can be found in the Supplemental Material [50].

III. RESULTS

Figure 1(d) displays M_5-edge VB RIXS data of UTe_2 in an energy range up to 12 eV for two incident energies, E_{res} (blue curves) and E_{res} - 4 eV (red curves). In addition to the elastic peak, we observe sharp peaks that we attribute to U $5f$ atomiclike multiplet excitations from the ground state (GS) of the type $5f^n_{GS} \rightarrow 5f^n_i$, and a broad shoulder which we associate with charge transfer scattering reaching $5f^{n+1}_j \underline{L}_j$ final states where $\underline{L}$ denotes a ligand hole. The multiplet excitations determine the leading $5f$ configuration in the mixed valent ground state as we will show below, and the charge transfer signal reflects the intermediate valent character of UTe_2. Figures 2(a)–2(f) presents experimental M_5- and M_4-edge VB-RIXS spectra in a smaller energy window of -0.5 to 2 eV of UGa_2, UCd_{11}, and UTe_2 for the same incident energies. UTe_2 data are compared to those from ferromagnetic UGa_2 ($T_C = 125$ K [51]), serving as a $5f^2$ reference material [46], and antiferromagnetic UCd_{11} ($T_N = 5.3$ K [52]), serving as a $5f^3$ reference [38,53]. The M_5 spectra are normalized to the most intense inelastic peak just above 1 eV energy transfer

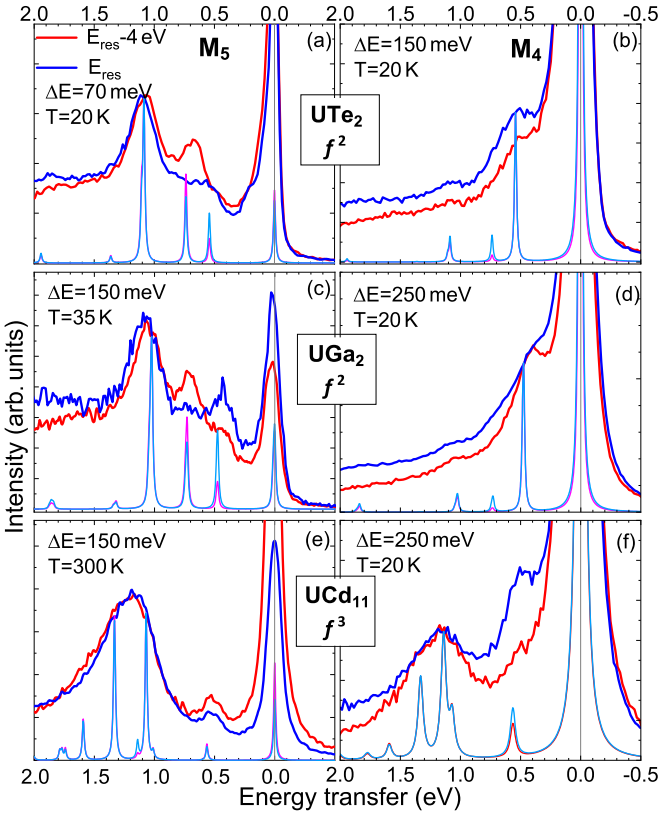

FIG. 2. (a)–(f) Valence band M-edge RIXS spectra for two different incident photon energies, at resonance E_{res} (blue, light blue) and at E_{res} - 4eV (red, magenta), for UTe_2 (a) and (b), UGa_2 (c) and (d), and UCd_{11} (e) and (f) at the M_5 (left) and M_4 edge (right), respectively. The thicker lines represent the data, the thinner lines the atomic multiplet calculations (see text).

without any background subtraction. Upon comparing the M_5 edges, we observe a prominent inelastic feature just above 1 eV in all samples, which appears broader and at slightly higher energy transfer in UCd_{11}. The M_5-edge RIXS data of UGa_2 and UTe_2 reveal two additional excitations below the strongest feature, whereas the UCd_{11} spectra in the lower energy region show only one less pronounced excitation. At the M_4 edge, the strong excitation above 1 eV persists only in the UCd_{11} data, while it is strongly suppressed in UGa_2 and UTe_2. As demonstrated below, the intensity suppression around 1 eV in the M_4 edge is a characteristic cross-section dependence for the $5f^2$ configuration.

RIXS spectra are simulated using full atomic multiplet calculations implemented in the *Quanty* code [54], starting with the atomic input values from the Atomic Structure Code by Cowan [55]. These values are reduced to account for covalence effects and configuration interaction, which are not included in the Hartree-Fock scheme [56–58]. Further information about the simulation can be found in the Supplemental Material [50].

Multiplet excitations are configuration specific so that they show at the same energy in the M_5 and M_4-edge RIXS spectra. However, cross sections may vary from edge to edge due to different quantum numbers involved. Consequently, the spectral weights of the respective multiplet excitations can differ significantly at the M_5 or M_4 edge. Indeed, simulations based on a U $5f^2$ configuration capture the suppression of spectral weight around 1 eV in the M_4-edge data compared to M_5 for UGa_2 and UTe_2 [see simulations in Figs. 2(a), 2(b), 2(c), and 2(d)]. Conversely, a simulation based on the $5f^3$ configuration would yield much more intensity in this energy range at the M_4 edge, as evident in Figs. 2(e) and 2(f) for UCd_{11}.

The good agreement between experimental and simulated cross-section dependence not only confirms the U $5f^2$ analysis of UGa_2 in Ref. [46], it also supports the assumption of Refs. [38,53] that UCd_{11} is a $5f^3$ compound. In contrast, UTe_2, akin to UGa_2, exhibits suppressed spectral weight of the multiplet structure around 1 eV when comparing the M_5 edge to the M_4 edge. Hence, we conclude that the M-edge RIXS spectra of UTe_2 resemble the multiplet structure of the $5f^2$ configuration, supporting the (less intense) $O_{4,5}$-edge RIXS data and analysis by Liu *et al.* [18].

IV. DISCUSSION

The presence of dominant local multiplet excitations in the $M_{4,5}$-edge RIXS spectra of UTe_2 is a direct signature of electronic correlations in the U $5f$ shell. However, the $5f^2$ character of the main local uranium configuration raises questions from a chemistry point of view because it implies that the U is formally 4+, suggesting all Te ions in UTe_2 should be formally 2−. A Te^{2-} ion is a notably large anion with an ionic radius of 2.21 Å [59]. For comparison, the Te-Te distance in EuTe (Eu^{2+}, Te^{2-}) is as large as 4.67 Å [60]. Examination of the Te-Te distances in UTe_2 reveals that only the Te1-Te1 distances of 4.123 Å are compatible with such a large ion. Te2 ions form chains along the b direction with Te2-Te2 distances of only 3.0355 Å [23] (see Fig. 1), which is too short to support a divalent state. These considerations were already put forward by Stöwe [61], who proposed the formal chemical charge state $U^{3+}Te_1^{2-}Te_2^{1-}$ if integer valences were to be used.

We performed density functional theory (DFT) calculations for UTe_2 to investigate the charge states of the noncorrelated, i.e., non-$5f$, states. The calculations were performed using the full potential local-orbital code (FPLO) [62], employing a local density approximation (LDA) (functional from Perdew and Wang [63]) in a full-relativistic approach that includes the spin orbit splitting (see the Supplemental Material for further details [50]). In Figs. 3 and 4, we highlight the $5p$ bands of Te1 (green) and Te2 (dark/light blue), and the $6d$ of U (gold/red). While the results for the correlated U $5f$ states require caution, the energy positions and dispersions of the broader Te $5p$ and U $6d$ bands can be reasonably trusted. In Fig. 3(a), all thick Te1 $5p$ bands lie 2 eV below the Fermi level, consistent with the formal charge of 2−. In contrast, Fig. 3(b) shows that parts of the Te2 $5p$ bands cross the Fermi level, exhibiting strong dispersion in the shaded regions that are cuts along the b direction [see the first Brillouin zone in Fig. 1(b)], in agreement with ARPES measurements along the $\overline{\Gamma}$-$\overline{Y}$ cuts [13]. These strongly dispersing bands are the Te2 $5p_y$ bands (highlighted in light blue), forming bonding and antibonding bands along the Te2 chains. Roughly half of these bands are below the Fermi level, and the other half is above E_F, as shown by the Te2 $5p_y$ partial density of states

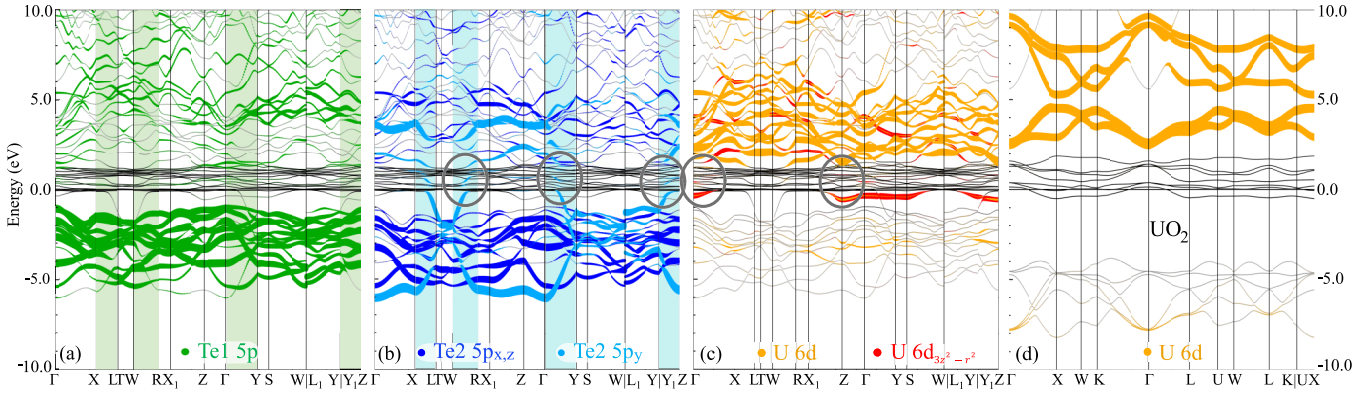

FIG. 3. Projected full relativistic band structure (DFT) of UTe_2 (a)–(c) and UO_2 (d) with U $5f$ states in black and the ones not explicitly highlighted in gray. $5p$ bands of Te1 (green) in (a), Te2 $5p_{x,y}$ (blue) and Te2 $5p_y$ bands (light blue) in (b), and U $6d_{3z^2-r^2}$ (red) and other U $6d$ states (gold) bands in (c). Shaded regions represent the high-symmetry cuts along b. The gray ellipses in (b) and (c) highlight regions of avoided crossing of Te2 $5p_y$ and U $5f$, and of U $6d_{3z^2-r^2}$ and U $5f$. Band structure of UO_2 with all U $6d$ bands in gold in (d).

(pDOS) in light blue in Fig. 4(b). These results support the notion of Te2 being 1− and not 2−, implying that one electron is donated from the Te2 $5p_y$ state to U.

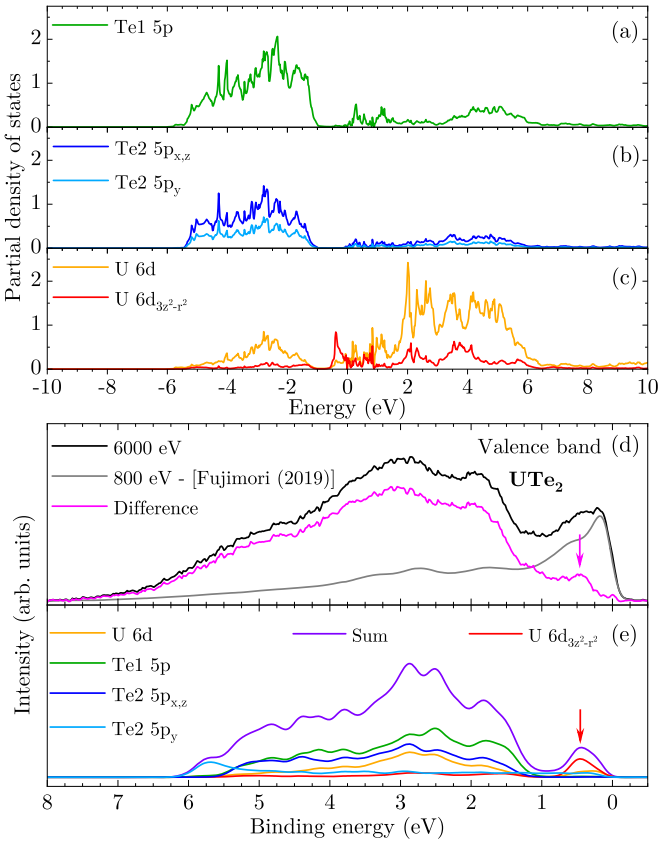

FIG. 4. (a)–(c) Partial density of states (DOS) corresponding to the band structure in Fig. 3. (d) Photoemission valence band data of UTe_2 measured with 6000 eV (black) and data at 800 eV (gray) as adapted from [12], and the difference plot (magenta) that no longer contains the $5f$ states. The arrow highlights the shallow peak around 0.5 eV. (e) Simulation of difference plot by adding up the respective partial DOSs from (a)–(c), weighted by their respective energy and shell-dependent photoionization cross sections (see text). The arrow indicates the enhanced U $6d_{3z^2-r^2}$ contribution at 0.5 eV.

Experimentally, though, we find the formal U $5f^2$ configuration in UTe_2. Hence, the donated electron must go somewhere else. Therefore, we explore the role of the U $6d$ states. For this, we compare the band structure of UTe_2 to that of UO_2, a well-studied semiconductor with a recognized U^{4+} $5f^2$ configuration [see Figs. 3(c) and 3(d)]. In UO_2, the $6d$ bands (gold) are situated well above the Fermi level, with very little $6d$ character below, confirming the local configuration of U in UO_2 as $5f^2 6d^0$. In contrast, UTe_2 exhibits the empty $6d$ bands (gold/red) much closer to the Fermi level, with a substantial amount of $6d$ character below the Fermi level. Notably, a filled $6d$ band (red) at around −0.5 eV has $3z^2$ - r^2 character and is the bonding part of the two $6d$ orbitals pointing toward each other along the U dimer parallel to the c axis. We conclude, the U $6d_{3z^2-r^2}$ absorbs the extra electron from Te2. Interestingly, this filled $6d_{3z^2-r^2}$ band is nonbonding concerning the Te1 and Te2 $5p$ bands, as evidenced from the absence of common characters or features in the bands and pDOS at −0.5 eV in Figs. 3(a)–3(c) and Figs. 4(a)–4(c).

The partial filling of the $6d_{3z^2-r^2}$ at −0.5 eV as derived from band structure is supported experimentally by photoelectron spectroscopy measurements of the valence band (VB) with hard (HAXPES) and soft x-rays (PES). In HAXPES, the cross section of the U $5f$ states is strongly reduced with respect to the U $6d$ and Te $5p$ states, whereas the U $5f$ states dominate the intensity in the PES spectra [64–70]. Hence, we can extract the non-f states using this strong photon energy dependence of the cross sections. Figure 4(d) displays the HAXPES VB data taken with 6000 eV x-rays (black curve) together with the cross-section corrected PES spectrum taken with 800 eV photons by Fujimori *et al.* [12] (gray curve). A detailed description of the HAXPES experimental set-up [71], adaption of the Fujimori data, and cross-section correction is given in the Supplemental Material [50]. The difference spectrum, see the magenta curve in Fig. 4(d), no longer contains contribution from the U $5f$ states. This spectrum is compared to the sum of the cross-section weighted pDOS of the U $6d$ (gold/red), Te1 (green), and Te2 (dark/light blue) $5p$, as shown in Fig. 4(e). The agreement between experiment and calculations is good, notably featuring a peak at 0.5 eV binding energy in the experiment (indicated by the magenta

arrow) that matches very well the peak in the U $6d_{3z^2-r2}$ pDOS (red arrow).

We note that the Te2 $5p_y$ bands are essentially nonbonding to the other Te $5p$ and U $6d$ bands. This is evident from the lack of common characters or features in Figs. 3(a)–3(c) and Figs. 4(a)–4(c). Thus, the Te2 $5p_y$ bands form a subsystem well separated from the rest. This indicates that the charge transfer of approximately one electron from Te2 $5p_y$ to U $6d_{3z^2-r2}$, which occurs through the conduction band, is unaffected by any potential charge transfer from the Te1 $5p$ and Te2 $5p_{x,z}$ to the U $6d$ bands as a result of hybridization.

Finally, we explore the role of the $5f$ states. In the calculations, the U $5f$ states are positioned around the Fermi level (black lines). Upon examining Figs. 3(a)–3(c), a noticeable avoidance of crossing is observed between these U $5f$ states and the Te2 $5p_y$ states, and even more so with the $6d_{3z^2-r^2}$ states [see the gray ellipses in Figs. 3(b) and 3(c)]. This suggests hybridization between Te2 $5p_y$ and U $5f$, as well as between U $6d_{3z^2-r^2}$ and U $5f$ bands. However, there is no evidence of direct hybridization between them because the respective avoided crossings in panels (b) and (c) are at different regions in k space. Therefore, the low-energy Hamiltonian of UTe_2 should commence with the local $5f^2$ configuration found in the RIXS experiment, the $5p_y$ states of the Te2 chains and the bonding states of the $6d_{3z^2-r2}$ orbitals in the U dimer.

V. CONCLUSION

In summary, high-resolution $M_{4,5}$-edge RIXS data of UTe_2 reveal atomiclike U $5f$-$5f$ excitations from the U $5f^2$ configuration, confirming the correlated nature of UTe_2 despite strong covalence and settling current debates concerning the dominating valence. The puzzle of the short Te2-Te2 distances, incompatible with formal U^{4+} valence, is resolved through band structure calculations and photon energy-dependent photoemission, showing charge transfer from $5p_y$ states of the Te2 chain is directed not to the U $5f$ but to the bonding state of the U $6d_{3z^2-r2}$ orbitals of the U dimer. Both hybridize with the U $5f$ states, so that the description of the physical properties of UTe_2 should include these two bands together with a $5f^2$ ansatz. We thus propose a scenario of partial entanglement of $5f$ states, involving a $5f^2$ configuration and some extra $5f$ electrons, likely forming bands or potentially participating in a Kondoesque manner.

ACKNOWLEDGMENTS

All authors thank Ulrich Burkhardt, Katharina Höfer, Anna Melendez-Sans, and Simone Altendorf for assistance with the sample preparation. A.S. acknowledges support from the German Research Foundation (DFG) Grant No. 387555779 and M.H. from the Bundesministerium für Bildung und Forschung (BMBF) - Grant No. 13K22XXB. All authors acknowledge DESY (Hamburg, Germany), a member of the Helmholtz Association HGF, for the provision of experimental facilities. Work at Los Alamos National Laboratory was performed under the auspices of the U.S. Department of Energy, Office of Basic Energy Sciences, Division of Materials Science and Engineering under project "Quantum Fluctuations in Narrow-Band Systems." M.M.B. acknowledges support from the Los Alamos Laboratory Directed Research and Development program. A.V.A. and L.H. benefited from financial support of the Czech Science Foundation Project No. 21-09766S. A.V.A. thanks further the Ferroic Multifunctionalities Project No. CZ.02.01.01/00/22_008/0004591. G.Z. acknowledges that this research was supported in part by Grant No. NSF PHY-2309135 to the Kavli Institute for Theoretical Physics (KITP).

[1] S. Ran, C. Eckberg, Q.-P. Ding, Y. Furukawa, T. Metz, S. R. Saha, I.-L. Liu, M. Zic, H. Kim, J. Paglione, and N. P. Butch, Nearly ferromagnetic spin-triplet superconductivity, Science **365**, 684 (2019).

[2] D. Aoki, A. Nakamura, F. Honda, D. Li, Y. Homma, Y. Shimizu, Y. J. Sato, G. Knebel, J.-P. Brison, A. Pourret, D. Braithwaite, G. Lapertot, Q. Niu, M. Vališka, H. Harima, and J. Flouquet, Unconventional superconductivity in heavy fermion UTe_2, J. Phys. Soc. Jpn. **88**, 043702 (2019).

[3] A. de Visser, UTe_2: A new spin-triplet pairing superconductor, JPSJ News and Comments **16**, 08 (2019).

[4] S. K. Lewin, C. E. Frank, S. Ran, J. Paglione, and N. P. Butch, A review of UTe_2 at high magnetic fields, Rep. Prog. Phys. **86**, 114501 (2023).

[5] I. M. Hayes, D. S. Wei, T. Metz, J. Zhang, Y. S. Eo, S. Ran, S. R. Saha, J. Collini, N. P. Butch, D. F. Agterberg, A. Kapitulnik, and J. Paglione, Multicomponent superconducting order parameter in UTe_2, Science **373**, 797 (2021).

[6] J. Ishizuka and Y. Yanase, Periodic Anderson model for magnetism and superconductivity in UTe_2, Phys. Rev. B **103**, 094504 (2021).

[7] K. Ishihara, M. Roppongi, M. Kobayashi, K. Imamura, Y. Mizukami, H. Sakai, P. Opletal, Y. Tokiwa, Y. Haga, K. Hashimoto, and T. Shibauchi, Chiral superconductivity in UTe_2 probed by anisotropic low-energy excitations, Nat. Commun. **14**, 2966 (2023).

[8] P. F. S. Rosa, A. Weiland, S. S. Fender, B. L. Scott, F. Ronning, J. D. Thompson, E. D. Bauer, and S. M. Thomas, Single thermodynamic transition at 2 K in superconducting UTe_2, Commun. Mater. **3**, 33 (2022).

[9] S. Suetsugu, M. Shimomura, M. Kamimura, T. Asaba, H. Asaeda, Y. Kosuge, Y. Sekino, S. Ikemori, Y. Kasahara, Y. Kohsaka, M. Lee, Y. Yanase, H. Sakai, P. Opletal, Y. Tokiwa, Y. Haga, and Y. Matsuda, Fully gapped pairing state in spin-triplet superconductor UTe_2 Sci. Adv. **10**, eadk3772 (2024).

[10] F. Theuss, A. Shragai, G. Grissonnanche, I. M. Hayes, S. R. Saha, Y. S. Eo, A. Suarez, T. Shishidou, N. P. Butch, J. Paglione, and B. J. Ramshaw, Single-component superconductivity in UTe_2 at ambient pressure, Nat. Phys. **20**, 1124, (2024).

[11] S. Lee, A. J. Woods, P. F. S. Rosa, S. M. Thomas, E. D. Bauer, S.-Z. Lin, and R. Movshovich, Anisotropic field-induced changes in the superconducting order parameter of UTe_2, arXiv:2310.04938.

[12] S.-i. Fujimori, I. Kawasaki, Y. Takeda, H. Yamagami, A. Nakamura, Y. Homma, and D. Aoki, Electronic structure of

UTe_2 studied by photoelectron spectroscopy, J. Phys. Soc. Jpn. **88**, 103701 (2019).

[13] L. Miao, S. Liu, Y. Xu, E. C. Kotta, C.-J. Kang, S. Ran, J. Paglione, G. Kotliar, N. P. Butch, J. D. Denlinger, and L. A. Wray, Low energy band structure and symmetries of UTe_2 from angle-resolved photoemission spectroscopy, Phys. Rev. Lett. **124**, 076401 (2020).

[14] S. M. Thomas, F. B. Santos, M. H. Christensen, T. Asaba, F. Ronning, J. D. Thompson, E. D. Bauer, R. M. Fernandes, G. Fabbris, and P. F. S. Rosa, Evidence for a pressure-induced antiferromagnetic quantum critical point in intermediate-valence UTe_2, Sci. Adv. **6**, eabc8709 (2020).

[15] S.-i. Fujimori, I. Kawasaki, Y. Takeda, H. Yamagami, A. Nakamura, Y. Homma, and D. Aoki, Core-level photoelectron spectroscopy study of UTe_2, J. Phys. Soc. Jpn. **90**, 015002 (2021).

[16] A. B. Shick, S.-I. Fujimori, and W. E. Pickett, UTe_2: A nearly insulating half-filled $j = \frac{5}{2} 5f^3$ heavy-fermion metal, Phys. Rev. B **103**, 125136 (2021).

[17] D. Aoki, H. Sakai, P. Opletal, Y. Tokiwa, J. Ishizuka, Y. Yanase, H. Harima, A. Nakamura, D. Li, Y. Homma, Y. Shimizu, G. Knebel, J. Flouquet, and Y. Haga, First observation of the de Haas–van Alphen effect and Fermi surfaces in the unconventional superconductor UTe_2, J. Phys. Soc. Jpn. **91**, 083704 (2022).

[18] S. Liu, Y. Xu, E. C. Kotta, L. Miao, S. Ran, J. Paglione, N. P. Butch, J. D. Denlinger, Y.-D. Chuang, and L. A. Wray, Identifying f-electron symmetries of UTe_2 with O-edge resonant inelastic x-ray scattering, Phys. Rev. B **106**, L241111 (2022).

[19] F. Wilhelm, J.-P. Sanchez, D. Braithwaite, G. Knebel, G. Lapertot, and A. Rogalev, Investigating the electronic states of UTe_2 using x-ray spectroscopy, Commun. Phys. **6**, 96 (2023).

[20] T. Shishidou, H. G. Suh, P. M. R. Brydon, M. Weinert, and D. F. Agterberg, Topological band and superconductivity in UTe_2, Phys. Rev. B **103**, 104504 (2021).

[21] T. Hazra and P. Coleman, Triplet pairing mechanisms from Hund's-Kondo models: Applications to UTe_2 and $CeRh_2As_2$, Phys. Rev. Lett. **130**, 136002 (2023).

[22] S. Khmelevskyi, L. V. Pourovskii, and E. A. Tereshina-Chitrova, Structure of the normal state and origin of the Schottky anomaly in the correlated heavy-fermion superconductor Ute_2, Phys. Rev. B **107**, 214501 (2023).

[23] V. Hutanu, H. Deng, S. Ran, W. T. Fuhrman, H. Thoma, and N. P. Butch, Low-temperature crystal structure of the unconventional spin-triplet superconductor UTe_2 from single-crystal neutron diffraction, Acta Crystallogr. Sect. B **76**, 137 (2020).

[24] H. Sakai, P. Opletal, Y. Tokiwa, E. Yamamoto, Y. Tokunaga, S. Kambe, and Y. Haga, Single crystal growth of superconducting UTe_2 by molten salt flux method, Phys. Rev. Mater. **6**, 073401 (2022).

[25] Z. Wu, T. I. Weinberger, J. Chen, A. Cabala, D. V. Chichinadze, D. Shaffer, J. Pospíšil, J. Prokleška, T. Haidamak, G. Bastien, V. Sechovský, A. J. Hickey, M. J. Mancera-Ugarte, S. Benjamin, D. E. Graf, Y. Skourski, G. G. Lonzarich, M. Vališka, F. M. Grosche, and A. G. Eaton, Enhanced triplet superconductivity in next-generation ultraclean UTe_2, Proc. Nat. Acad. Sci. USA **121**, e2403067121 (2024).

[26] H. Matsumura, H. Fujibayashi, K. Kinjo, S. Kitagawa, K. Ishida, Y. Tokunaga, H. Sakai, S. Kambe, A. Nakamura, Y. Shimizu, Y. Homma, D. Li, F. Honda, and D. Aoki, Large reduction in the a-axis knight shift on UTe_2 with $T_c = 2.1$ k, J. Phys. Soc. Jpn. **92**, 063701 (2023).

[27] G. Knebel, W. Knafo, A. Pourret, Q. Niu, M. Vališka, D. Braithwaite, G. Lapertot, M. Nardone, A. Zitouni, S. Mishra, I. Sheikin, G. Seyfarth, J.-P. Brison, D. Aoki, and J. Flouquet, Field-reentrant superconductivity close to a metamagnetic transition in the heavy-fermion superconductor UTe_2, J. Phys. Soc. Jpn. **88**, 063707 (2019).

[28] S. Ran, I.-L. Liu, Y. S. Eo, D. J. Campbell, P. M. Neves, W. T. Fuhrman, S. R. Saha, C. Eckberg, H. Kim, D. Graf, F. Balakirev, J. Singleton, J. Paglione, and N. P. Butch, Extreme magnetic field-boosted superconductivity, Nat. Phys. **15**, 1250 (2019).

[29] W. Knafo, T. Thebault, P. Manuel, D. D. Khalyavin, F. Orlandi, E. Ressouche, K. Beauvois, G. Lapertot, K. Kaneko, D. Aoki, D. Braithwaite, G. Knebel, and S. Raymond, Incommensurate antiferromagnetism in UTe_2 under pressure, arXiv:2311.05455.

[30] S. Ran, H. Kim, I.-L. Liu, S. R. Saha, I. Hayes, T. Metz, Y. S. Eo, J. Paglione, and N. P. Butch, Enhancement and reentrance of spin triplet superconductivity in UTe_2 under pressure, Phys. Rev. B **101**, 140503 (2020).

[31] L. Q. Huston, D. Y. Popov, A. Weiland, M. M. Bordelon, P. F. S. Rosa, R. L. Rowland, B. L. Scott, G. Shen, C. Park, E. K. Moss, S. M. Thomas, J. D. Thompson, B. T. Sturtevant, and E. D. Bauer, Metastable phase of UTe_2 formed under high pressure above 5 GPa, Phys. Rev. Mater. **6**, 114801 (2022).

[32] F. Honda, S. Kobayashi, N. Kawamura, S. I. Kawaguchi, T. Koizumi, Y. J. Sato, Y. Homma, N. Ishimatsu, J. Gouchi, Y. Uwatoko, H. Harima, J. Flouquet, and D. Aoki, Pressure-induced structural phase transition and new superconducting phase in UTe_2, J. Phys. Soc. Jpn. **92**, 044702 (2023).

[33] H.-H. Kung, R. E. Baumbach, E. D. Bauer, V. K. Thorsmølle, W.-L. Zhang, K. Haule, J. A. Mydosh, and G. Blumberg, Chirality density wave of the hidden order phase in URu_2Si_2, Science **347**, 1339 (2015).

[34] A. Marino, D. S. Christovam, D. Takegami, J. Falke, M. M. F. Carvalho, T. Okauchi, C.-F. Chang, S. G. Altendorf, A. Amorese, M. Sundermann, A. Gloskovskii, H. Gretarsson, B. Keimer, A. V. Andreev, L. Havela, A. Leithe-Jasper, A. Severing, J. Kuneš, L. H. Tjeng, and A. Hariki, Quantifying the U $5f$ covalence and degree of localization in U intermetallics, Phys. Rev. Res. **6**, 033068 (2024).

[35] J. R. Jeffries, K. T. Moore, N. P. Butch, and M. B. Maple, Degree of $5f$ electron localization in URu_2Si_2: Electron energy-loss spectroscopy and spin-orbit sum rule analysis, Phys. Rev. B **82**, 033103 (2010).

[36] S.-i. Fujimori, T. Ohkochi, I. Kawasaki, A. Yasui, Y. Takeda, T. Okane, Y. Saitoh, A. Fujimori, H. Yamagami, Y. Haga, E. Yamamoto, Y. Tokiwa, S. Ikeda, T. Sugai, H. Ohkuni, N. Kimura, and Y. Onuki, Electronic structure of heavy fermion uranium compounds studied by core-level photoelectron spectroscopy, J. Phys. Soc. Jpn. **81**, 014703 (2012).

[37] L. A. Wray, J. Denlinger, S. W. Huang, H. He, N. P. Butch, M. B. Maple, Z. Hussain, and Y. D. Chuang, Spectroscopic determination of the atomic f-electron symmetry underlying hidden order in URu_2Si_2, Phys. Rev. Lett. **114**, 236401 (2015).

[38] C. H. Booth, S. A. Medling, J. G. Tobin, R. E. Baumbach, E. D. Bauer, D. Sokaras, D. Nordlund, and T.-C. Weng, Probing $5f$-state configurations in URu_2Si_2 with U L_{III}-edge resonant x-ray emission spectroscopy, Phys. Rev. B **94**, 045121 (2016).

[39] M. Sundermann, M. W. Haverkort, S. Agrestini, A. Al-Zein, M. Moretti Sala, Y. Huang, M. Golden, A. de Visser, P. Thalmeier, L. H. Tjeng, and A. Severing, Direct bulk-sensitive probe of $5f$ symmetry in URu_2Si_2, Proc. Nat. Acad. Sci. USA **113**, 13989 (2016).

[40] K. O. Kvashnina, H. C. Walker, N. Magnani, G. H. Lander, and R. Caciuffo, Resonant x-ray spectroscopy of uranium intermetallics at the $M_{4,5}$ edges of uranium, Phys. Rev. B **95**, 245103 (2017).

[41] F. Wilhelm, J. P. Sanchez, and A. Rogalev, Magnetism of uranium compounds probed by XMCD spectroscopy, J. Phys. D: Appl. Phys. **51**, 333001 (2018).

[42] G. van der Laan and B. T. Thole, X-ray-absorption sum rules in jj-coupled operators and ground-state moments of actinide ions, Phys. Rev. B **53**, 14458 (1996).

[43] G. van der Laan, K. T. Moore, J. G. Tobin, B. W. Chung, M. A. Wall, and A. J. Schwartz, Applicability of the spin-orbit sum rule for the actinide $5f$ states, Phys. Rev. Lett. **93**, 097401 (2004).

[44] G. van der Laan, private communication (2024).

[45] E. L. Bright, L. Xu, L. M. Harding, R. Springell, A. C. Walters, M. Sundermann, M. Garcia-Fernandez, S. Agrestini, R. Caciuffo, G. van der Laan, and G. H. Lander, Resonant inelastic x-ray scattering from U_3O_8 and UN, J. Phys.: Cond. Mat. **35**, 175501 (2023).

[46] A. Marino, M. Sundermann, D. S. Christovam, A. Amorese, C.-F. Chang, P. Dolmantas, A. H. Said, H. Gretarsson, B. Keimer, M. W. Haverkort, A. V. Andreev, L. Havela, P. Thalmeier, L. H. Tjeng, and A. Severing, Singlet magnetism in intermetallic UGa_2 unveiled by inelastic x-ray scattering, Phys. Rev. B **108**, 045142 (2023).

[47] D. Ketenoglu, M. Harder, K. Klementiev, M. Upton, M. Taherkhani, M. Spiwek, F.-U. Dill, H.-C. Wille, and H. Yavaş, Resonant inelastic X-ray scattering spectrometer with 25meV resolution at the Cu K-edge, J. Synchrotron Rad. **22**, 961 (2015).

[48] A. H. Said, T. Gog, M. Wieczorek, X. Huang, D. Casa, E. Kasman, R. Divan, and J. H. Kim, High-energy-resolution diced spherical quartz analyzers for resonant inelastic X-ray scattering, J. Synchrotron Radiat. **25**, 373 (2018).

[49] H. Gretarsson, D. Ketenoglu, M. Harder, S. Mayer, F.-U. Dill, M. Spiwek, H. Schulte-Schrepping, M. Tischer, H.-C. Wille, B. Keimer, and H. Yavaş, IRIXS: a resonant inelastic x-ray scattering instrument dedicated to X-rays in the intermediate energy range, J. Synchrotron Rad. **27**, 538 (2020).

[50] See Supplemental Material at http://link.aps.org/supplemental/10.1103/PhysRevResearch.6.033299 for further information on sample preparation & quality, experimental set-ups, simulations, band structure calculations, and cross-section analysis.

[51] A. Lawson, A. Williams, J. Smith, P. Seeger, J. Goldstone, J. O'Rourke, and Z. Fisk, Magnetic neutron diffraction study of UGa_3 and UGa_2, J. Magn. Magn. Mater. **50**, 83 (1985).

[52] E. Yamamoto, Y. Hirose, K. Enoki, K. Mitamura, K. Sugiyama, T. Takeuchi, M. Hagiwara, K. Kindo, Y. Haga, R. Settai, and Y. Onuki, Heavy fermion state in antiferromagnet UCd_{11}, J. Phys. Soc. Jpn. **81**, SB023 (2012).

[53] A. Amorese, M. Sundermann, B. Leedahl, A. Marino, D. Takegami, H. Gretarsson, A. Gloskovskii, C. Schlueter, M. W. Haverkort, Y. Huang, M. Szlawska, D. Kaczorowski, S. Ran, M. B. Maple, E. D. Bauer, A. Leithe-Jasper, P. Hansmann, P. Thalmeier, L. H. Tjeng, and A. Severing, From antiferromagnetic and hidden order to Pauli paramagnetism in UM_2Si_2 compounds with $5f$ electron duality, Proc. Natl. Acad. Sci. USA **117**, 30220 (2020).

[54] M. W. Haverkort, *Quanty* for core level spectroscopy - excitons, resonances and band excitations in time and frequency domain, J. Phys.: Conf. Ser. **712**, 012001 (2016).

[55] R. D. Cowan, *The Theory of Atomic Structure and Spectra* (University of California Press, Berkeley and Los Angeles, 1981).

[56] A. Tanaka and T. Jo, Resonant 3*d*, 3*p* and 3*s* photoemission in transition metal oxides predicted at 2*p* threshold, J. Phys. Soc. Jpn. **63**, 2788 (1994).

[57] F. de Groot and A. Kotani, *Core Level Spectrocopy of Solis*, Advances in Condensed Matter Science (CRC Press, Boca Raton, 2008), Vol. 6.

[58] S. Agrestini, C.-Y. Kuo, M. Moretti Sala, Z. Hu, D. Kasinathan, K.-T. Ko, P. Glatzel, M. Rossi, J.-D. Cafun, K. O. Kvashnina, A. Matsumoto, T. Takayama, H. Takagi, L. H. Tjeng, and M. W. Haverkort, Long-range interactions in the effective low-energy hamiltonian of Sr_2IrO_4: A core-to-core resonant inelastic x-ray scattering study, Phys. Rev. B **95**, 205123 (2017).

[59] V. Jović, Tellurium, *Geochemistry*, Encyclopedia of Earth Science (EESS) (Springer, Dordrecht, Netherlands, 1998), pp. 621–622.

[60] M. Lafrentz, D. Brunne, B. Kaminski, V. V. Pavlov, A. B. Henriques, R. V. Pisarev, D. R. Yakovlev, G. Springholz, G. Bauer, E. Abramof, P. H. O. Rappl, and M. Bayer, Optical third-harmonic spectroscopy of the magnetic semiconductor EuTe, Phys. Rev. B **82**, 235206 (2010).

[61] K. Stöwe, Uncommon valence states in the metallic lanthanide and actinide diiodides MI_2 (M=La, Ce, Nd, Gd and Th) and in the uranium tellurides UTe_2, U_2Te_5 and UTe_3 Part 2: the uranium tellurides UTe_2, U_2Te_5 and α-UTe_3, J. Alloys Compd. **246**, 111 (1997).

[62] K. Koepernik and H. Eschrig, Full-potential nonorthogonal local-orbital minimum-basis band-structure scheme, Phys. Rev. B **59**, 1743 (1999).

[63] J. P. Perdew and Y. Wang, Accurate and simple analytic representation of the electron-gas correlation energy, Phys. Rev. B **45**, 13244 (1992).

[64] M. B. Trzhaskovskaya, V. I. Needov, and V. G. Yarzhemsky, Photoelectron angular distribution parameters for elements $Z = 1$ to $Z = 54$ in the photoelectron energy range 100–5000 eV, At. Data Nucl. Data Tables **77**, 97 (2001).

[65] M. B. Trzhaskovskaya, V. I. Needov, and V. G. Yarzhemsky, Photoelectron angular distribution parameters for elements $Z = 55$ to $Z = 100$ in the photoelectron energy range 100–5000 eV, At. Data Nucl. Data Tables **82**, 257 (2002).

[66] M. B. Trzhaskovskaya, V. K. Nikulin, V. I. Nefedov, and V. G. Yarzhemsky, Non-dipole second order parameters of the photoelectron angular distribution for elements $Z = 1$–100 in the photoelectron energy range 1–10 keV, At. Data Nucl. Data Tables **92**, 245 (2006).

[67] H. Rosner, J. Gegner, D. Regesch, W. Schnelle, R. Gumeniuk, A. Leithe-Jasper, H. Fujiwara, T. Haupricht, T. C. Koethe, H.-H. Hsieh, H.-J. Lin, C. T. Chen, A. Ormeci, Y. Grin, and L. H. Tjeng, Electronic structure of $SrPt_4Ge_{12}$: Combined photoelectron spectroscopy and band structure study, Phys. Rev. B **80**, 075114 (2009).

[68] D. Takegami, L. Nicolaï, T. C. Koethe, D. Kasinathan, C. Y. Kuo, Y. F. Liao, K. D. Tsuei, G. Panaccione, F. Offi, G. Monaco, N. B. Brookes, J. Minár, and L. H. Tjeng, Valence band hard x-ray photoelectron spectroscopy on 3*d* transition-metal oxides containing rare-earth elements, Phys. Rev. B **99**, 165101 (2019).

[69] D. Takegami, C.-Y. Kuo, K. Kasebayashi, J.-G. Kim, C. F. Chang, C. E. Liu, C. N. Wu, D. Kasinathan, S. G. Altendorf, K. Hoefer, F. Meneghin, A. Marino, Y. F. Liao, K. D. Tsuei, C. T. Chen, K.-T. Ko, A. Günther, S. G. Ebbinghaus, J. W. Seo, D. H. Lee *et al.*, $CaCu_3Ru_4O_{12}$: A high-Kondo-temperature transition-metal oxide, Phys. Rev. X **12**, 011017 (2022).

[70] S. G. Altendorf, D. Takegami, A. Meléndez-Sans, C. F. Chang, M. Yoshimura, K. D. Tsuei, A. Tanaka, M. Schmidt, and L. H. Tjeng, Electronic structure of the Fe^{2+} compound $FeWO_4$: A combined experimental and theoretical x-ray photoelectron spectroscopy study, Phys. Rev. B **108**, 085119 (2023).

[71] C. Schlueter, A. Gloskovskii, K. Ederer, I. Schostak, S. Piec, I. Sarkar, Y. Matveyev, P. Lömker, M. Sing, R. Claessen, C. Wiemann, C. M. Schneider, K. Medjanik, G. Schönhense, P. Amann, A. Nilsson, and W. Drube, The new dedicated HAXPES beamline P22 at PETRA III, AIP Conf. Proc. **2054**, 040010 (2019).